Title
Metasurface terahertz laser with electronically-controlled polarization

ISBN
9781943580279

Authors
Chen, D
Xu, L
Curwen, CA
et al.

Publication Date
2017-10-25

DOI
10.1364/CLEO_AT.2017.FTu4G.5

Peer reviewed

Metasurface quantum-cascade laser with electrically-switchable polarization

LUYAO XU,[1,2,†] DAGUAN CHEN,[1,†] CHRISTOPHER A. CURWEN,[1,2] MOHAMMAD MEMARIAN,[1] JOHN L. RENO,[3] TATSUO ITOH,[1] AND BENJAMIN S. WILLIAMS[1,2,*]

[1]*Department of Electrical Engineering, University of California, Los Angeles, CA 90095, USA*
[2]*California NanoSystems Institute, University of California, Los Angeles, CA 90095, USA*
[3]*Sandia National Laboratories, Center of Integrated Nanotechnologies, MS 1303, Albuquerque, NM 87185, USA*
**Corresponding author: bswilliams@ucla.edu*

Received XX Month XXXX; revised XX Month, XXXX; accepted XX Month XXXX; posted XX Month XXXX (Doc. ID XXXXX); published XX Month XXXX

Dynamic control of a laser's output polarization state is desirable for applications in polarization sensitive imaging, spectroscopy, and ellipsometry. Using external elements to control the polarization state is a common approach. Less common and more challenging is directly switching the polarization state of a laser, which, however, has the potential to provide high switching speed, compactness and power efficiency. Here, we demonstrate a new approach to achieve direct and electrically-controlled polarization switching of a semiconductor laser. This is enabled by integrating a polarization-sensitive metasurface with semiconductor gain medium to selectively amplify a cavity mode with the designed polarization state, therefore leading to an output in the designed polarization. Here the demonstration is for a terahertz quantum-cascade laser, which exhibits electrically-controlled switching between two linear polarization separated by 80°, while maintaining an excellent beam with narrow divergence of ~3°×3°, single-mode operation fixed at ~3.4 THz, combined with a peak power as high as 93 mW at a temperature of 77 K. The polarization-sensitive metasurface is composed of two interleaved arrays of surface emitting antennas, all of which are loaded with quantum-cascade gain materials. Each array is designed to resonantly interact with one specific polarization; when electrical bias is selectively applied to the gain material in one array, selective amplification of one polarization occurs. The amplifying metasurface is used along with an output coupler reflector to build a vertical-external-cavity surface-emitting-laser (VECSEL), whose output polarization state can be switched solely electrically. This work demonstrates the potential of exploiting amplifying polarization-sensitive metasurfaces to create lasers with desirable polarization states — a concept which is applicable beyond the terahertz and can potentially be applied to shorter wavelengths. © 2016 Optical Society of America

OCIS codes: *(130.5440) Polarization-selective devices; (140.5965) Semiconductor lasers, quantum cascade; (140.7270) Vertical emitting lasers ; (260.5430) Polarization; (160.3918) Metamaterials.*

http://dx.doi.org/10.1364/XXXXXXXX

1. INTRODUCTION

The ability to control the polarization state of light from a laser is fundamental, as well as being desirable for a variety of applications, including polarization sensitive imaging, measurements of Faraday rotation, and circular dichroism spectroscopy. Typically, external elements (e.g. polarizers and waveplates) are used to control polarization – less common is the direct switching of the polarization state of the laser itself. Classical methods of changing the polarization direction of lasers generally rely on mechanical means such as movable optics or electromechanical piezo components [1-3], which are bulky and expensive. One exception is in some VCSELs which exhibit optical bistability and can be switched between nearly degenerate orthogonally polarized modes using injection current [4, 5]. However, since the dependence upon injection current can be hard to predict, injection locking or an adjustable external cavity is often needed to improve stability [6-8]. Meanwhile, several passive metamaterial/metasurface structures have displayed the ability to select a specific circular polarization using chiral plasmonic structures [9-11]. A compact semiconductor laser with dynamic polarization control capability integrated on chip is desirable, especially in the terahertz (THz) range where many basic optical components are not readily available.

There have been several efforts to engineer the polarization of quantum-cascade lasers. In the mid-IR, plasmonic polarizers have been integrated onto the QC-laser facet to generate linear or circularly polarized light [12]; in another case a modified ridge waveguide acted as a TM to TE polarization mode converter [13]. In the THz region, circularly polarized emission from a THz QC-laser has been obtained by patterning surface emitting gratings comprising sets of orthogonally oriented slots [14]. However, these are essentially static devices, with the polarization determined at the time of fabrication. To our knowledge, only two examples of dynamic polarization tuning of a QC-laser have been demonstrated: one instance in which a TE to TM waveguide mode converter was biased to tune linear polarization over 45 degrees [15], and one instance in which two side-by-side and ~$\pi/2$ phased-shifted QC-lasers feed surface emitting gratings composed of orthogonally oriented antennas, which demonstrated linear to near-circular polarization tuning controlled by the current injection difference between the two lasers [16]. Nevertheless, dynamic modulation of THz polarization still mostly relies on external modulator

elements, such as rotating polarizers/waveplates [17], active THz metamaterials [11, 18, 19], and liquid crystal based waveplates [20, 21], all of which are subject to insertion loss and modulation speed limits. Photoelastic techniques for rapid polarization modulation are not available at THz frequencies. In this paper, we report a THz QC-laser with built-in electrically-controlled polarization switching between linear polarization states, obtained while maintaining high output power, a single-mode spectrum, and an excellent beam pattern, all of which are nearly unaffected as the polarization is switched.

The foundation of this work is our recently demonstrated metasurface-based QC-VECSELs, which exhibit simultaneous high-power/efficiency and excellent beam quality [22, 23]. The enabling component of a QC-VECSEL is the active reflectarray metasurface, which is made up of an array of low quality-factor resonant antennas. Each antenna sub-cavity is a metal-metal waveguide loaded with electrically-biased QC active material, so that the incident THz radiation is coupled in, amplified, and re-radiated. The active metasurface provides a highly flexible platform for integrating new functionality into a QC-laser. In this work, we design a metasurface based around interleaved sets of cross-polarized antennas, a concept which has been previously demonstrated in the microwave range using leaky-wave antennas [24]. Fig. 1(a) shows an SEM image of a fabricated polarization-selective metasurface. It is most intuitive to consider each "zigzag" antenna as a set of patch antennas that couple to the incident electric field polarized along the patch width (13 μm in this case), and are resonant at a frequency that corresponds approximately to when the width is equal to half of the wavelength within the semiconductor. Sets of patches are rotated either at an angle of 45° or 135° from the x-axis; these patches are then connected by narrower segments needed to allow a continuous dc injection current path for each antenna (as seen in Fig. 1(a)). Patches of one orientation type are all electrically connected to one wire bonding area and thus can be biased separately from the other type. By switching the electrical bias between the two sets, we can select the polarization preference that the metasurface amplifies and reflects. By pairing such a metasurface with an output coupler that is insensitive to polarization (see Fig. 1(b)), we create a QC-VECSEL with electrically-controlled polarization switching capability. Because the cavity mode profile doesn't depend upon the detailed antenna structure, high power and excellent beam pattern can be consistently maintained as polarization is switched.

2. DESIGN

The design goal for the metasurface is straightforward: first, when injection current is applied to a single set of antennas we wish to obtain net reflectance gain at a narrow range of frequencies for a single incident polarization (i.e. $|\Gamma_{45°\text{-}45°}| > 1$, while $|\Gamma_{135°\text{-}135°}| < 1$ when Set 1 is biased and Set 2 is unbiased). Second, to ensure polarization purity, we must suppress cross-polarized scattering at those same frequencies ($|\Gamma_{45°\text{-}135°}| \approx |\Gamma_{135°\text{-}45°}| \approx 0$). Fig. 1(c) shows a top view of the metasurface design and dimensions. Due to their geometry, Set 1 patches (drawn in darker blue) respond to light polarized at 135°, while Set 2 patches respond to light polarized at 45°. These patches, appearing as the thicker portion of the zigzags (13 μm wide), have width of approximately $\lambda/2n$, where λ is the free space wavelength of designed frequency, and n is the index of refraction in the GaAs/AlGaAs quantum-well medium. The period is 71 μm in the horizontal direction and approximately 46.1 μm in the vertical direction (with the exact value being a function of the patch length of 39 μm, the connector width of 6.4 μm, and the right angle they form). The periodicity of the metasurface is chosen to be sufficiently small to avoid Bragg scattering at 3.4 THz for normally incident waves.

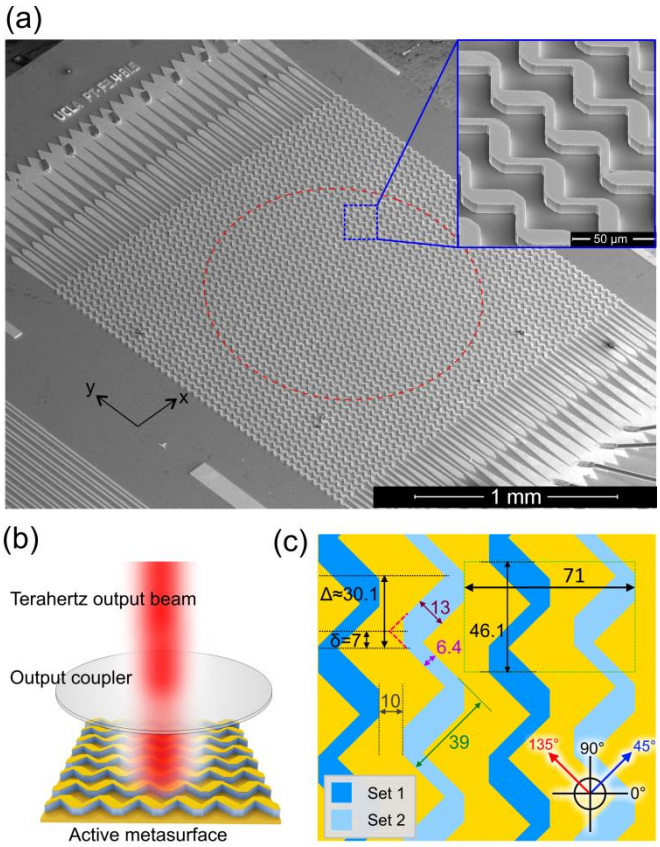

Fig. 1. (a) An SEM image of the fabricated metasurface. The zigzag metasurface covers an area of 2 × 2 mm^2. Only a center circular region of 1.5 mm diameter is biased, shown by the red dashed circle. The portions outside the circle have a SiO_2 layer beneath the top metallization to prevent the quantum well medium from being biased. The tapered terminations serve both as the wire bonding region and help suppress reflection of traveling waveguide modes to prevent self-lasing. Antennas preferring one polarization direction are electrically connected together through the tapers on the top left of the metasurface, while others preferring the orthogonal polarization direction are connected together on the bottom right side. The inset shows a zoom-in SEM image. (b) A schematic of the plano-plano VECSEL cavity. (c) Top view of a portion of the metasurface illustrated with dimensions given in microns. One set of antennas - the ones interacting with radiation linearly polarized at 45° - is shown in dark blue, while the second set of antennas, which interacts with radiation linearly polarized at 135°, is shown in light blue. For brevity, the former set will be referred to as Set 1, while the latter will be referred to as Set 2. The region inside the green dashed rectangular is one unit cell.

While the concept of using rotated sets of patch antennas is straightforward, the detailed implementation has several subtleties involved with minimizing the effect of the connector segments needed to provide a continuous top metallization, and with preventing cross-coupling between the two sets of antennas. First, cross-polarization scattering is reduced by clipping off the right-angled "elbow" bends along the zigzags, shown as dashed red lines in the upper corner of Fig. 1(c). Second, we suppress cross-coupling between adjacent, separately biased antennas by introducing a vertical offset $\Delta \approx 30.1$ μm (with exact value being a sum of the variable $\delta = 7$ μm defined in Fig. 1(c) and a geometric constant rounded to 23.1 μm). Zero offset leads to a structure with adjacent ridges being mirror images with respect to the y-axis (i.e. 90° axis shown in Fig. 1(c)). The value of the offset and amount of clipping has been optimized by parametric study of the effect of each parameter on the amount of cross-coupling, using single-cell periodic simulations (see Supplement 1 for details on simulations with different offset values), with the goal to suppress the unwanted cross-polarized

scattering (i.e. ensure $|\Gamma_{45°\text{-}135°}| \approx |\Gamma_{135°\text{-}45°}| \approx 0$) to ensure the purity of generated linear polarization.

Modeling was performed using full-wave 3D finite-element simulations (Ansys HFSS). Reflection mode simulations at normal incidence were performed for a unit cell using periodic boundary conditions to simulate infinitely periodic arrays. The Drude model was used to describe the free carrier scattering loss in GaAs/AlGaAs material and gold metallization (free carrier density used for metal is 5.9×10^{22} cm^{-3} and for active medium is 5×10^{19} cm^{-3}. Drude lifetime used for metal is 39 fs and active medium is 0.5 ps). The QC-laser material gain coefficient g was modeled using an anisotropic permittivity, and was assumed to be frequency independent over the simulation range. For clarity, we define gain coefficients g_1 and g_2 to represent the mount of gain supplied to Set 1 and Set 2 patches respectively. Fig. 2(a) shows the simulated co-polarization and cross-polarization reflectance $|\Gamma_{ij}|^2$ of the metasurface for two cases: the metasurface is passive ($g_1 = g_2 = 0$) as well as the case where Set 1 patches only are supplied with a gain of g_1 = 30 cm^{-1} (emulating "turning on" Set 1 patches using bias current) and Set 2 patches kept passive ($g_2 = 0$). When gain is supplied to Set 1 only, net gain is observed for incident E-field polarized at 45° near the target frequency of 3.4 THz, while the orthogonal polarization 135° is almost unchanged compared to the fully passive case. A closer investigation of reflectance change against gain in Set 1 at 3.4 THz confirms the effectiveness of selectively amplifying one specific polarization via the bias switch (see Fig. 2(c)); indeed, examination of the E-field profile show the field mostly localized to the Set 1 antennas. Furthermore, the design shows high effectiveness in suppressing cross-polarization near the target frequency ($|\Gamma_{45°\text{-}135°}|^2$ and $|\Gamma_{135°\text{-}45°}|^2 < 0.01$ across a bandwidth of 51 GHz). The asymmetric reflectance lineshape is likely a characteristic of a Fano resonance owing to the interactions and coupling paths between the complex set of resonances present within the metasurface lattice. One consequence of this is the strong cross-polarization scattering seen at 3.48 THz, particularly when gain is applied (see Supplement 1 for the field profile at 3.48 THz).

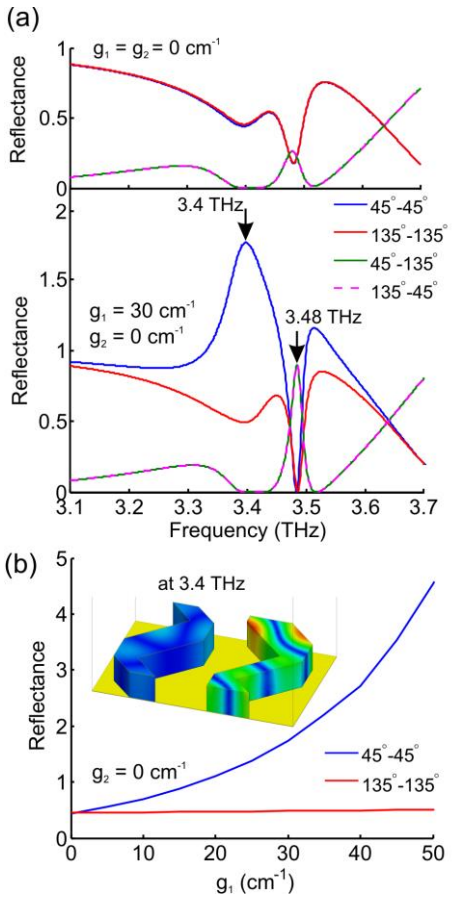

Fig. 2. (a) Top: Co-polarization and cross-polarization reflectance of the metasurface when Set 1 and Set 2 are both passive. The 45°-45° reflectance $|\Gamma_{45°\text{-}45°}|^2$ designates the reflectance of light linearly polarized at 45° (defined according to the coordinates given in Fig. 1(c)) into light linearly polarized at 45°, and so on. Bottom: Co-polarization and cross-polarization reflectance of the metasurface when a QC gain of g_1 = 30 cm^{-1} is assumed for Set 1 patches and Set 2 is kept passive. (b) The peak reflectance for 45°-45°and 135°-135° reflectance plotted against the gain g_1 supplied to Set 1 with Set 2 kept passive throughout. Inset is the simulated E-field intensity pattern of a unit cell at 3.4 THz for an incident E-field polarized at 45°.

The expected polarization state of this laser is calculated by applying the polarization repeatability to the cavity round-trip propagation matrix, i.e. $\gamma\vec{E} = \Gamma_M\vec{E}$, where the matrices for the output coupler, free space and the cryostat window are ignored since they have no effect on the polarization. The metasurface field reflection matrix Γ_M is defined as

$$\Gamma_M = \begin{bmatrix} \Gamma_{45^\circ\text{-}45^\circ} & \Gamma_{45^\circ\text{-}135^\circ} \\ \Gamma_{135^\circ\text{-}45^\circ} & \Gamma_{135^\circ\text{-}135^\circ} \end{bmatrix} \quad \textbf{(1)}$$

and the values are obtained from the simulated complex reflection spectrum (see Supplement 1 for simulated reflection phase data). We are able to predict the cavity polarization eigenstate $\vec{E}$ by calculating the eigenvector of Γ_M. γ is the eigenvalue associated with the eigenvector, representing the reflection amplitude experienced by the solved polarization eigenstate. At the resonant frequency of 3.40 THz, the calculated polarization ellipses exhibits linear polarization with a high E-field intensity axial ratio of 55 dB; furthermore, we expect the two possible bias states to produce beams whose polarization direction is separated by 89.2°, as illustrated in Fig. 3(a). However, if the laser is forced to oscillate away from the reflectance peak for any reason, we can expect increased cross-polarization scattering, and decreased orthogonality. This is shown by calculating the expected eigenstate for operating frequencies approximately 13 GHz below and above the resonant frequency in Fig. 3(b)(c); the polarization becomes slightly elliptically polarized, with the intensity axial ratios decreased to 26.2 dB and 28.1 dB respectively, as well as 6° - 15° deviation in the angular separation between two bias states.

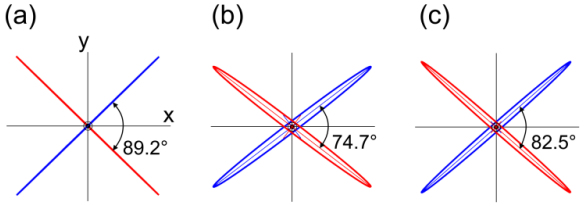

Fig. 3. (a) The simulated polarization eigenstate ellipses for the output beam when operating at the peak reflectance frequency of 3.397 THz. The two selectable polarization states, shown in blue (Set 1 switched on) and red (Set 2 switched on), differ by a rotation of 89.2° and the intensity axial ratio of the ellipse's major axis to its minor axis is 55 dB for both. (b) The polarization eigenstate ellipse for the output beam when operating at 3.384 THz. and 3.41 THz are plotted in (b) and (c). For these calculations, the co-polarized reflectance is held constant at its value at 3.397 THz in order to simulate all three cases with the same lasing threshold, with only the cross-polarized reflectance varied.

We terminate the patch arrays with lossy tapers to suppress any self-lasing of antenna ridges in propagating mode, similar to the previous metasurface designs [24, 25]. Additionally, to ensure that self-lasing of the antenna sub-cavity doesn't occur before the VECSEL lasing, we performed 3D Floquet-Bloch eigenmode finite-element simulations including both radiative and material losses, to ensure that there were no high quality factor modes close in frequency to the design frequency.

3. FABRICATION AND CAVITY SETUP

A resonant phonon depopulation active region design very similar to [25] around 3.4 THz is used in this work, which was grown by molecular beam epitaxy in the GaAs/$Al_{0.15}Ga_{0.85}As$ material system (wafer number VB0739). The fabrication of polarimetric metasurface followed the standard procedures for making metal-metal waveguides such as described in Ref. [26]. The 10 μm-thick QC active layer was bonded to a receiving GaAs wafer via Cu-Cu thermocompression bonding, followed by substrate removal. Then a layer of 200 nm-thick SiO_2 layer was deposited and patterned to provide insulation between the top metal contact and the active region in the area outside the red circle as shown in Fig. 1(a), including taper, wire-boding area, and part of the array area. A Ti/Au/Ni metal layer was evaporated and lifted off to provide both top metallization and self-aligned etch mask for the subsequent Chlorine-based dry etching to define the ridges. Finally, the Ni was etched away, and Ti/Au was evaporated onto the wafer backside. Dies are then cleaved and indium soldered to a Cu heat spreader.

The demonstrated VECSEL is based on a plano-plano Fabry-Perot cavity defined by the polarimetric metasurface mounted inside a cryostat and an output coupler in parallel mounted externally. The cryostat has a 3-mm-thick high-resistivity silicon window that introduces an intracavity etalon filter effect. The cavity length is approximately 9 mm. The output coupler used here is an inductive metal mesh on a 100 μm-thick crystal quartz substrate, whose transmission is approximately 20% around 3.4 THz (see Supplement 1 for the measured transmission spectrum).

4. RESULTS ON POLARIZATION-SWITCHABLE VECSEL

Electrical, power, and spectral characteristics were evaluated for a fixed VECSEL cavity alignment, where Set 1 and Set 2 antennas were switched on one at a time. As shown in Fig. 4, pulsed power-current-voltage (*P-I-V*) curves were measured at 77 K for each set with 0.25% overall duty cycle (500 ns-long pulses repeated at 10 kHz, modulated by a 150 Hz pulse train with lock-in detection). The power is measured using a pyroelectric detector and calibrated by a Thomas-Keating THz absolute power meter with 100% collection efficiency (given the directive beam pattern achieved). The measured *P-I-V* curves are very similar for the two sets, both exhibiting a threshold current density of 420 A/cm^2, a slope efficiency of 190 mW/A, and a peak power of ~93 mW. For comparison, a conventional metal-metal waveguide fabricated from the same wafer during the same process run had a threshold current density of 330 A/cm^2 at 77 K (see Supplement 1). Single-mode lasing operation was observed for both sets at an identical frequency of 3.37 THz (within the FTIR spectrometer's resolution of 7.5 GHz), which did not change with electrical bias.

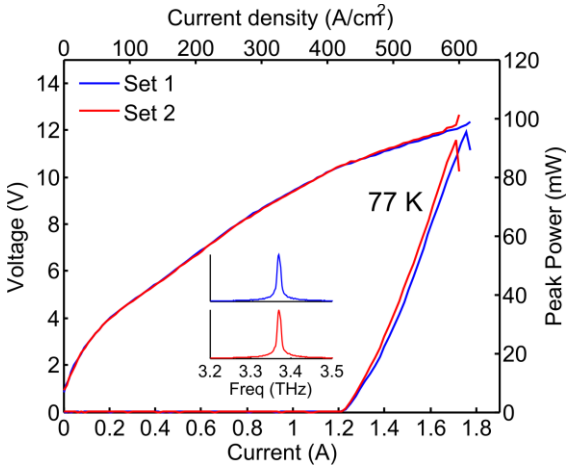

Fig. 4. Pulsed *P-I-V* curves measured for Set 1 and Set 2 in the same cavity setup at 77 K. The inset is the spectra measured for the two sets.

To analyze the polarization state of the output, we placed a wire-grid polarizer (Infraspecs model P03) in between the output coupler and the detector, and measured the power as the polarizer is rotated. This measurement was conducted for Set 1 and Set 2 by switching on one set at a time. The results shown in Fig. 5(a) demonstrates a polarization switching between linear polarized states separated by 80°. The slight deviation from the ideal value of 90° is likely due to non-ideal cross-polarized scattering from the metasurface, the reasons for which are discussed below. Far-field beam patterns were characterized using a 2-axis spherical scanning pyroelectric detector for Set 1 and Set 2 at the same bias point near the maximum power output. As it can be seen in Fig. 5(b)-(e), the measured beams are almost identical as the bias is switched between 2 sets, both exhibiting a directive and narrow near-Gaussian pattern with full-width-half-maximum (FWHM) angular divergence of ~3°×3°. Hence, the electrically-controlled polarization switching is conducted without significantly affecting the output beam, spectrum, or total power.

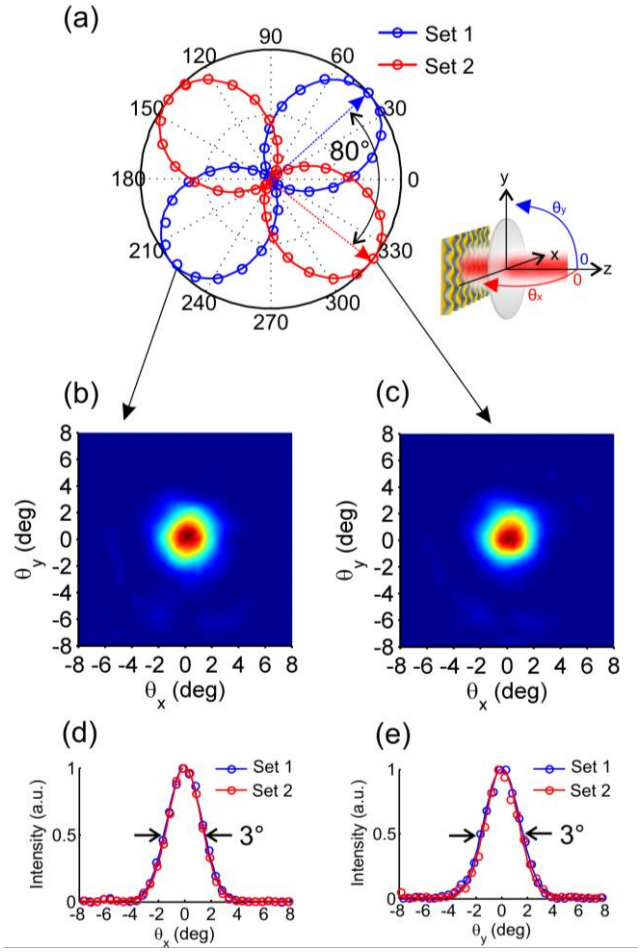

Fig. 5. (a) The measured total power through the polarizer versus the polarizer angle for two sets. 80° linear polarization angle switching is shown in arrow. Circles are experimental data, and the solid lines in red and blue are the fitting curves (to Eq. (2)). The schematic on the bottom right of (a) shows the 2-axis far-field beam pattern measurement scheme. The measured 2D beam patterns for Set 1 and Set 2 are shown in (b) and (c), with an angular resolution of 0.5°. The 1D cuts along x and y directions through the beam center for Set 1 and Set 2 are plotted in colored circle in (d) and (e), with the Gaussian curve fitting results plotted in solid colored lines.

The uniformity of polarization over the beam was further evaluated by measuring the power vs. polarizer orientation at different beam spots. Fig. 6 presents the mapping results at five different beam spots, including one at the center and the other four that are 2° away from the

center in four directions. It can be seen that the polarization is very uniform across the x-axis. It is slightly less uniform across the y axis with a maximum deviation of 22° for Set 1 and 13° for Set 2 rotated towards the y-axis. We further assessed the linear polarization purity by fitting the power against polarizer angle data to the expression:

$$I = a_0(T_s + T_p) + a_1(T_s - T_p)\cos(2\theta_p - 2\varphi) \quad \textbf{(2)}$$

where a_0, a_1, and φ are the fitting parameters, and θ_p is the varying angle that the axis of the polarizer makes with respect to the 0° direction. The derivation of this formula is detailed in Supplement 1. T_s and T_p are respectively the wire-grid polarizer's transmittance for electric field polarized crossed and parallel to the wires' direction, the values of which in THz range are $T_s = 0.8$ and $T_p = 10^{-4}$. The linear polarization purity is evaluated by the intensity ratio between the dominant polarization and the cross polarization of obtained as $\frac{a_0 + a_1}{a_0 - a_1}$. This value is ideally infinite for pure linear polarization. The extracted intensity axial ratios for the total beam and five beam spots are listed in Table 1, which are all greater than 10 dB. The purity level is lowest at Spot 3 on the beam pattern for both sets, which suggests that the cross-polarized field component induced by the cross-polarization scattering on the metasurface is out-of-phase with the dominant polarized field, leading to slight elliptical polarization. We believe that this moderate amount of polarization non-uniformity, including the linear polarization rotation and slight elliptical polarization, can be attributed to the not fully suppressed cross-polarized reflection on the metasurface. Two major factors could lead to an increased strength of cross-polarization. First, the lasing frequency likely has some deviation from the ideal resonance frequency of the fabricated metasurface. As detailed in Design section above, a slight deviation of the VECSEL lasing frequency away from the designed metasurface resonance frequency of 3.4 THz can result in a slightly elliptically polarized beam and a deviation of angular separation from the ideal value of 90°. An exact match between is difficult to achieve in experiment, since the lasing frequency is determined by a combination of factors, including the cryostat window's etalon filter effect (with a free spectral range of 13 GHz), the active medium gain profile, and the metasurface resonance peak. The effects of this frequency deviation on cross-polarized scattering may be exacerbated by the fact that the metasurface dimensions are slightly smaller than design (i.e. a 0.5-μm change in the patch width) due to photolithography. Second, enhanced cross-polarized scattering may also result from the obliquely incident field component in the Gaussian cavity mode profile, which was not accounted for in our simulation of normal incidence plane waves.

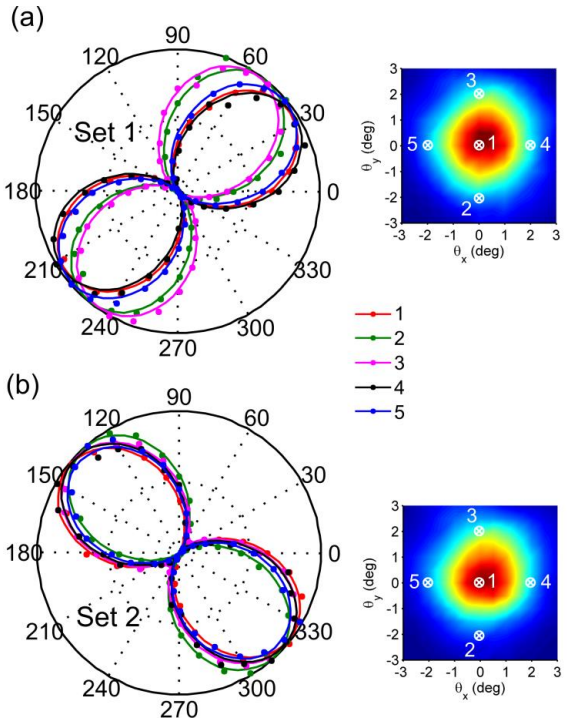

Fig. 6. Measured power through the polarizer against the polarizer angle at five spots on the output beam for Set 1 (a) and Set 2 (b). Dots are experimental data, and the solid lines in are the fitting curves (to Eq. (2)).

Table 1. Axial ratios of field intensity (in unit of dB) for the total beam and different beam spots from Set 1 and Set 2 patches

	Total beam	1	2	3	4	5
Set 1	16.5	15.4	17.7	12.1	24.5	20.4
Set 2	13.8	18.3	30	10.7	15.2	22.9

5. RESULTS ON METASURFACE SELF-LASING

The metasurface QC-VECSEL is designed to operate with only one antenna set switched on at a time. Nonetheless, a natural question arises — what if both antenna sets are switched on together? For example, might one be able to continuously vary the polarization of the output state as in the case of passive cross-polarized antennas? Unfortunately the answer is no – due to cross coupling between antennas sets, introduction of gain into both sets significantly changes the reflectance spectrum, and results in lasing at different frequencies than the original design at 3.40 THz. However this behavior is interesting in its own right.

In experiment, when both sets of antennas were biased together, we observed self-lasing of the metasurface alone without any output coupler. The measured *P-I-V* curve and spectra at different biases are shown in Fig. 7(a). Single-mode lasing at a frequency of 3.75 THz is observed, and is unchanged with bias within the resolution of the FTIR. The power peaks at 144 mW with a slope efficiency estimated at 139 mW/A. The threshold current density is 400 A/cm^2, lower than the threshold for the polarimetric VECSEL, although the larger bias area results in a larger total threshold current. The power output is in the surface normal direction and exhibits a directive and narrow beam of 3°×4° FWHM divergence, as shown in Fig. 7(b), which is measured with the metasurface positioned as the origin of the measurement setup as Fig. 5(a) shows. Some excess power below the main lobe is observed; we speculate that this may result from scattering from the wire bonds. The polarization over the output beam is found to be largely linearly over the beam, but with a very non-uniform distribution of polarization direction, as shown in Fig. 7(c). We speculate that this behavior is associated with the complex and spatially varying phase relation

between the coupled modes in Set 1 and Set 2, along with inhomogeneities in fabrication, structure, and biasing which break the expected symmetry between 45°- and 135°-polarized radiation. This is not fully understood, and will require further detailed simulation and experimental study.

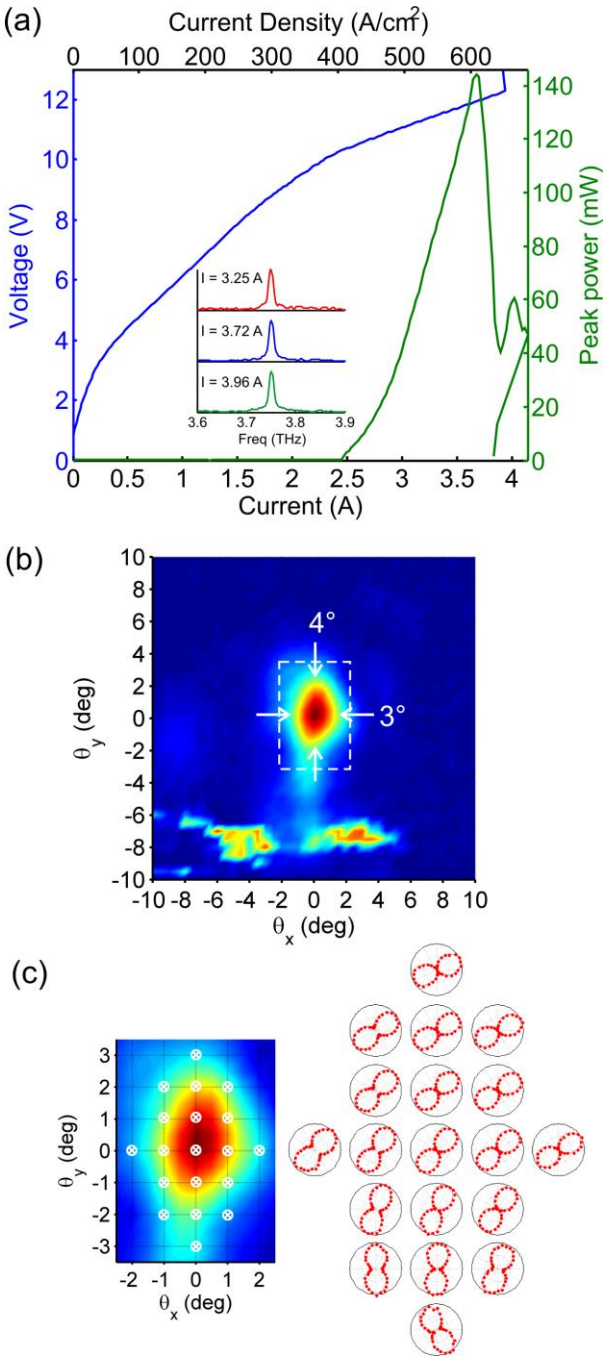

Fig. 7. (a) Measured *P-I-V* curve for the polarimetric metasurface without an external cavity. Nominally identical bias is provided to both Set 1 and Set 2. The inset shows the spectra at different injection current levels. (b) Measured far-field beam pattern for the metasurface self-lasing near the peak power, with FWHM divergence angles in x and y direction labeled. The polarization is mapped at different beam spots within the white dashed box. (c) Measured power through the polarizer at different spots on the beam pattern indicated by the circle white cross marks.

The self-lasing phenomenon is consistent with behavior predicted both by eigenmode type simulations and driven reflection mode simulations if both antenna sets are supplied with the same amount of gain (see Supplement 1 for details on simulation results). The simulated reflectance spectra shows the emergence of a sharp Fano-type resonance at 3.80 THz for $g_1 = g_2 = 20$ cm^{-1} in both the co- and cross-polarization reflectance. The eigenmode simulation shows that the metasurface exhibits self-lasing in a surface emitting mode at ~3.8 THz with a low threshold gain of ~17 cm^{-1} (see Supplement 1 for details on simulated gain threshold for several modes found between 3 - 4 THz). This gain threshold is lower than the value of 28 cm^{-1} estimated for the metasurface VECSEL lasing. This self-lasing is attributed to a standing wave mode resonance along the antenna patch length; the mode is "bright" in that it radiates strongly in the far field with even parity. If only one set is biased, simulations predict that the gain threshold is much larger – approximately 30 - 35 cm^{-1}.

This self-lasing phenomenon can be considered to be an unintentional realization of a laser array phase-locked through mutual antenna coupling, similar to that reported in Ref. [27]. The self-lasing mode relies on strong coupling between sets of antennas, as is revealed by the strong cross-polarized scattering shown in simulation results at 3.80 THz, and the fact that the gain threshold is much higher when only one set of antennas is biased (Fig. S5 and Fig. S6 in Supplement 1). The fact that such a narrow far-field beam was obtained indicates that locking is obtained over the entire 1.5-mm diameter bias area (19 wavelengths), which encompasses ~1080 patch elements. The performance of this self-lasing phenomenon could be further improved, if the metasurface was designed by intention to bring the self-lasing frequency down to better match the QC material optimal gain region of 3.3 - 3.5 THz.

6. CONCLUSION

We have demonstrated a THz metasurface QC-laser with electrically-switchable polarization. Dynamic switching of the linear polarization angle of the laser between two states separated by 80° is observed, while maintaining consistent high output power, threshold, single-mode spectrum, and a high quality beam pattern. This represents the flexibility of the metasurface QC-VECSEL approach to customize the polarization response. Such a polarization-switchable terahertz laser is relatively simple to assemble, and offers compactness, robustness, and speed over other designs that use moving parts. Furthermore, because our approach is based upon switching of gain within a laser cavity, it avoids issues with insertion loss associated with external polarimetric modulators, which can be particularly large in the THz region. Indeed, there doesn't appear to be a significant performance penalty of this device compared to conventional QC-VECSELs [23]. In addition, polarization purity is observed to be greater than 13 dB for the total output, and the polarization state is mostly uniform across different positions within the beam pattern – it is likely this can be further improved by optimization of the VECSEL cavity have the lasing frequency better match the metasurface resonance, and exploration of advanced metasurface designs with improved broadband suppression of cross-polarized scattering. The biasing may also be switched with a high modulation frequency: in principle the switching speed is limited only by the build-up time of the laser oscillation (~nanosecond or less), and the RC time constant associated with the electrical bias. Such a high-performance QC-laser with electrically-switchable polarization may find use within a multitude of terahertz applications, such as polarimetry, spectroscopy, and cancer detection [28-30]. Furthermore, simply by adding a quarter-waveplate in the path of the output beam, the laser can be converted into one which switches between circular polarizations of opposite handedness. Or alternately a future chiral metasurface design could selectively amplify specific circular polarization states directly.

Finally it is important to comment upon the prospects for continuous-wave (cw) operation for the polarimetric metasurface laser architecture. The devices reported here were tested at low duty-cycle. The large bias area (1.5-mm diameter) draws a great deal of current; as a result the total thermal load is too large to allow cw operation at 77 K. However, we would emphasize that the metasurface VECSEL

architecture is very advantageous for cw or high-duty cycle operation once the bias area is reduced to bring down the total thermal load. In particular, the narrow ridge geometry of each antenna is an advantageous geometry for heat removal. For example, in separate work 40 mW cw power at 6 K was observed from a QC-VECSEL with a 1-mm bias area diameter [23], and 5 - 7 mW of cw power at 83 K was reported in a QC-VECSEL with a 0.7-mm bias area diameter [31].

Funding. National Science Foundation (NSF) (1150071, 1407711, 1610892), National Aeronautics and Space Administration (NASA) (NNX16AC73G).

Acknowledgment. Microfabrication was performed at the UCLA Nanoelectronics Research Facility, and wire bonding was performed at the UCLA Center for High Frequency Electronics. This work was performed, in part, at the Center for Integrated Nanotechnologies, an Office of Science User Facility operated for the U.S. Department of Energy (DOE) Office of Science. Sandia National Laboratories is a multi-program laboratory managed and operated by Sandia Corporation, a wholly owned subsidiary of Lockheed Martin Corporation, for the U.S. Department of Energy's National Nuclear Security Administration under contract DE-AC04-94AL85000.

†These authors contributed equally to this work.

See Supplement 1 for supporting content.

REFERENCES

1. R. J. Zhou, B. Ibarra-Escamilla, J. W. Haus, P. E. Powers, and Q. W. Zhan, "Fiber laser generating switchable radially and azimuthally polarized beams with 140 mW output power at 1.6 μm wavelength," Appl. Phys. Lett. **95**, 191111 (2009).
2. O. B. Yu, J. L. Cruz, and M. V. Andres, "Polarization switchable Erbium-doped all-fiber laser," Laser Phys. Lett. **5**, 676 (2008).
3. A. Fraser, M. Bernier, J.-D. Deschênes, É. Weynant, J. Genest, and R. Vallée, "Polarization-switchable Q-switched DFB fiber laser," Opt. Lett. **35**, 1046 (2010).
4. K. D. Choquette, D. A. Richie, and R. E. Leibenguth, "Temperature-Dependence of Gain-Guided Vertical-Cavity Surface-Emitting Laser Polarization," Appl. Phys. Lett. **64**, 2062 (1994).
5. K. D. Choquette, K. L. Lear, R. P. Schneider, and R. E. Leibenguth, "Gain-Dependent Polarization Properties of Vertical-Cavity Lasers," 14th IEEE International Semiconductor Laser Conference, 149 (1994).
6. T. H. Russell, and T. D. Milster, "Polarization switching control in vertical-cavity surface-emitting lasers," Appl. Phys. Lett. **70**, 2520 (1997).
7. K. D. Choquette, K. L. Lear, R. E. Leibenguth, and M. T. Asom, "Polarization Modulation of Cruciform Vertical-Cavity Laser-Diodes," Appl. Phys. Lett. **64**, 2767 (1994).
8. M. Torre, A. Hurtado, A. Quirce, A. Valle, L. Pesquera, and M. Adams, "Polarization Switching in Long-Wavelength VCSELs Subject to Orthogonal Optical Injection," IEEE J. Quantum Electron. **47**, 92 (2011).
9. V. A. Fedotov, A. S. Schwanecke, N. I. Zheludev, V. V. Khardikov, and S. L. Prosvirnin, "Asymmetric transmission of light and enantiomerically sensitive plasmon resonance in planar chiral nanostructures," Nano Lett. **7**, 1996 (2007).
10. E. Plum, and N. I. Zheludev, "Chiral mirrors," Appl. Phys. Lett. **106** (2015).
11. T. Kan, A. Isozaki, N. Kanda, N. Nemoto, K. Konishi, H. Takahashi, M. Kuwata-Gonokami, K. Matsumoto, and I. Shimoyama, "Enantiomeric switching of chiral metamaterial for terahertz polarization modulation employing vertically deformable MEMS spirals," Nat. Commun. **6** (2015).
12. N. F. Yu, Q. J. Wang, C. Pflugl, L. Diehl, F. Capasso, T. Edamura, S. Furuta, M. Yamanishi, and H. Kan, "Semiconductor lasers with integrated plasmonic polarizers," Appl. Phys. Lett. **94**, 151101 (2009).
13. D. Dhirhe, T. J. Slight, B. M. Holmes, D. C. Hutchings, and C. N. Ironside, "Quantum cascade lasers with an integrated polarization mode converter," Opt. Express **20**, 25711 (2012).
14. P. Rauter, J. Lin, P. Genevet, S. P. Khanna, M. Lachab, A. G. Davies, E. H. Linfield, and F. Capasso, "Electrically pumped semiconductor laser with monolithic control of circular polarization," Proc. Natl. Acad. Sci. USA (2014).
15. D. Dhirhe, T. J. Slight, B. M. Holmes, and C. N. Ironside, "Active polarisation control of a quantum cascade laser using tuneable birefringence in waveguides," Opt. Express **21**, 24267 (2013).
16. G. Liang, T. Liu, and Q. J. Wang, "Recent Developments of Terahertz Quantum Cascade Lasers," IEEE J. Sel. Topics Quantum Electron. **23**, 1 (2017).
17. G. S. Jenkins, D. C. Schmadel, and H. D. Drew, "Simultaneous measurement of circular dichroism and Faraday rotation at terahertz frequencies utilizing electric field sensitive detection via polarization modulation," Rev. Sci. Instrum. **81**, 083902 (2010).
18. X. G. Peralta, I. Brener, W. J. Padilla, E. W. Young, A. J. Hoffman, M. J. Cich, R. D. Averitt, M. C. Wanke, J. B. Wright, H.-T. Chen, J. F. O'Hara, A. J. Taylor, J. Waldman, W. D. Goodhue, J. Li, and J. Reno, "External modulators for terahertz quantum cascade lasers based on electrically-driven active metamaterials," Metamaterials **4**, 83 (2010).
19. G. D. Metcalfe, M. Wraback, A. Strikwerda, K. Fan, X. Zhang, and R. Averitt, "Terahertz Polarimetry Based on Metamaterial Devices," Proc. SPIE **8363**, 83630O (2012).
20. C. F. Hsieh, R. P. Pan, T. T. Tang, H. L. Chen, and C. L. Pan, "Voltage-controlled liquid-crystal terahertz phase shifter and quarter-wave plate," Opt. Lett. **31**, 1112 (2006).
21. C. S. Yang, T. T. Tang, P. H. Chen, R. P. Pan, P. S. Yu, and C. L. Pan, "Voltage-controlled liquid-crystal terahertz phase shifter with indium-tin-oxide nanowhiskers as transparent electrodes," Opt. Lett. **39**, 2511 (2014).
22. L. Xu, C. A. Curwen, P. W. C. Hon, Q.-S. Chen, T. Itoh, and B. S. Williams, "Metasurface external cavity laser," Appl. Phys. Lett. **107**, 221105 (2015).
23. L. Xu, D. Chen, T. Itoh, J. L. Reno, and B. S. Williams, "Focusing metasurface quantum-cascade laser with a near diffraction-limited beam," Opt. Express **24**, 24117 (2016).
24. Y. D. Dong, and T. Itoh, "Substrate Integrated Composite Right-/Left-Handed Leaky-Wave Structure for Polarization-Flexible Antenna Application," IEEE Trans. Antennas Propag **60**, 760 (2012).
25. L. Li, L. Chen, J. Zhu, J. Freeman, P. Dean, A. Valavanis, A. G. Davies, and E. H. Linfield, "Terahertz quantum cascade lasers with >1 W output powers," Electron. Lett. **50**, 309 (2014).
26. B. S. Williams, S. Kumar, Q. Hu, and J. L. Reno, "Operation of terahertz quantum-cascade lasers at 164 K in pulsed mode and at 117 K in continuous-wave mode," Opt. Express **13**, 3331 (2005).
27. T. Y. Kao, J. L. Reno, and Q. Hu, "Phase-locked laser arrays through global antenna mutual coupling," Nat. Photon. **10**, 541 (2016).
28. P. Doradla, K. Alavi, C. Joseph, and R. Giles, "Single-channel prototype terahertz endoscopic system," J. Biomed. Opt. **19** (2014).
29. K. Mochizuki, M. Aoki, S. R. Tripathi, and N. Hiromoto, "Polarization-changeable THz time-domain spectroscopy system with a small incident-angle beam-splitter," 2009 34th International Conference on Infrared, Millimeter, and Terahertz Waves, Vols 1 and 2, 690 (2009).
30. P. Doradla, K. Alavi, C. S. Joseph, and R. H. Giles, "Terahertz polarization imaging for colon cancer detection," in *Proc. SPIE 8985, Terahertz, RF, Millimeter, and Submillimeter-Wave Technology and Applications VII*(2014), pp. 89850K.
31. L. Xu, C. A. Curwen, J. L. Reno, T. Itoh, and B. S. Williams, "High performance THz metasurface quantum cascade lasers with an intra-cryostat cavity," (manuscript in preparation) (2017).